Available online at www.sciencedirect.com
SCIENCE DIRECT®
Journal of Solid State Chemistry 178 (2005) 2913–2921
JOURNAL OF SOLID STATE CHEMISTRY
www.elsevier.com/locate/jssc

$Mn(HPO_3)$: A new manganese (II) phosphite with a condensed structure

U-Chan Chung[a], José L. Mesa[b,*], José L. Pizarro[a], Veronique Jubera[c], Luis Lezama[b], María I. Arriortua[a], Teófilo Rojo[b,*]

[a]*Departamento de Mineralogía y Petrología, Facultad de Ciencia y Tecnología, Universidad del País Vasco, Apdo. 644, E-48080, Bilbao, Spain*
[b]*Departamento de Química Inorgánica, Facultad de Ciencia y Tecnología, Universidad del País Vasco, Apdo. 644, E-48080, Bilbao, Spain*
[c]*ICMCB, CNRS [UPR 9048], Université Bordeaux I, 87 av. du Dr. Schweitzer, 33608 Pessac cedex, France*

Received 2 May 2005; received in revised form 17 June 2005; accepted 21 June 2005

Abstract

A new manganese (II) phosphite with the formula $Mn(HPO_3)$ has been synthesised under mild hydrothermal conditions and autogenous pressure. Large pink coloured single crystals were obtained, allowing the resolution of the structure by x-ray diffraction. $Mn(HPO_3)$ crystallises in the $P2_1/c$ monoclinic space group with $a = 8.036(3)$ Å, $b = 8.240(3)$ Å, $c = 10.410(3)$ Å, $\beta = 124.73(3)^\circ$ and $Z = 8$. The structure consists of a three-dimensional, compact framework of edge sharing MnO_6 octahedra linked to phosphite groups via oxygens. The presence of the phosphite anion has been confirmed by IR spectroscopy. $Mn(HPO_3)$ presents a high thermal stability limit of 580 °C, before rapid transformation to $Mn_2P_2O_7$ occurs. Photoluminescence and diffuse reflectance spectroscopy studies show the presence of high spin Mn(II) in significantly distorted octahedral coordination with Dq and Racah parameters of Dq = 820, $B = 910$ and $C = 3135\,cm^{-1}$. The ESR spectra, performed at different temperatures, are isotropic with a g-value of 2.00(1). Magnetic measurements indicate global antiferromagnetic interactions with a ferromagnetic transition at 15 K, attributed to a canting of the antiferromagneticaly aligned spins.

Keywords: Hydrothermal synthesis; X-ray diffraction; UV/v is and luminescent spectroscopies; Magnetic behavior

1. Introduction

Materials science has been growing very fast in recent decades, giving rise to an incredible number of new phases with a non-less amazing chemical diversity. The design of condensed phases which can give rise to original physical properties, by making use of the great number of different cations and arrangements that they can exhibit, is an important area in this field [1].

Since Bonavia et al. obtained the first organically templated phosphite with open framework [2], the phosphite oxo-anion $(HPO_3)^{2-}$, has been the source of many new hybrid inorganic–organic phosphites [3]. Condensed phosphites, however, are scarce compared with the number of organically templated structures containing this group. Cations used to synthesise these compounds are diverse and go from alkali metals to group 14 of the periodic table through transition metals and there are even some examples with rare earth elements. Most of these condensed phases were reported in the 1980s and 1990s and were only studied structurally [4]. The high versatility of the phosphite group to form new structures is due to its pyramidal morphology that allows it to display properties of both tetrahedral and triangular oxo-anionic groups.

In this paper we present the hydrothermal synthesis, crystal structure determination and the thermal, luminescent

*Corresponding authors. Fax: +34 946013500.
E-mail addresses: qipmeruj@lg.ehu.es (J.L. Mesa), qiproapt@lg.ehu.es (T. Rojo).

0022-4596/$ - see front matter © 2005 Elsevier Inc. All rights reserved.
doi:10.1016/j.jssc.2005.06.038

and magnetic behavior of a new condensed manganese (II) phosphite, $Mn(HPO_3)$.

2. Experimental section

2.1. Synthesis and characterisation

$Mn(HPO_3)$ has been synthesised under mild hydrothermal conditions and autogenous pressure. H_3PO_3 (12.2 mmol), $MnCl_2 \cdot 4H_2O$ (1.0 mmol) and ethanol (87.4 mmol) were dissolved in distilled water (20 mL) whilst stirring. Tripropylamine (10.5 mmol) was added prior to sealing the mixture in a PTFE-lined stainless steel pressure vessel. The pH value could not be determined due to the insolubility of the organic molecule in water. The interphase formed between tripropylamine and the aqueous solution presents the ideal conditions where $Mn(HPO_3)$ crystallises. After 5 days at 170 °C, the vessel was slowly cooled to room temperature. Large, light pink coloured crystals were separated by filtration, washed with water and acetone and dried in air, the yield being approximately 85%.

Density of a single crystal was measured by the flotation [5] method using a mixture of bromoform (Br_3CH, $\rho = 2.82\,g\,cm^{-3}$) and diiodomethane (CH_2I_2, $\rho = 3.32\,g\,cm^{-3}$), obtaining an experimental density $\rho_{exp} = 3.15(3)\,g\,cm^{-3}$. Manganese and phosphorus contents were measured by inductively coupled plasma atomic emission spectroscopy (ICP-AES) with values of Mn: 40.2% and P: 22.6% (required Mn: 40.7% and P: 23%). The infrared spectrum shows bands corresponding to the vibrational modes of the phosphite group. Table 1 contains the values of the band assignation. These values are similar to those found in the literature for the $(HPO_3)^{2-}$ anion [2,3a,3b,3c,3g,3m6].

2.2. Single crystal X-ray diffraction study

A prismatic single-crystal with dimensions $0.3 \times 0.25 \times 0.2$ mm, was selected under a polarising microscope and mounted on a glass fibre. Single-crystal X-ray diffraction data were collected at room temperature on an Oxford Diffraction XCALIBUR2 automated diffractometer (Mo-$K\alpha$ radiation) equipped with a CCD detector. The Lorentz-Polarisation and absorption corrections were made with the diffractometer software, taking into account the size and shape of the crystal [7]. The structure was solved by direct methods (SIR 92) [8] in the monoclinic $P2_1/c$ space group, and refined by full matrix least-squares based on F^2, using SHELXL 97 [9]. Scattering factors were taken from Ref. [10]. Table 2 contains details of crystal data, data collection process and some features of structure refinement. The hydrogen atoms belonging to the phosphite group were not initially found but located in the difference Fourier map. Anisotropic thermal parameters were refined for all atoms except hydrogen, which were refined isotropically. All structure drawings were made using the ATOMS program [11]. The crystallographic data have been deposited at the Cambridge Structural Database (CSD No. 414646).

Table 1
Band assignment for the $Mn(HPO_3)$ infrared spectrum

Position (cm^{-1})	Assignment
2443, 2430 (m)	ν (P–H)
1155 (s)	ν_{as} (PO_3)
1075, 1045 (m)	δ (P–H)
988, 970 (s)	ν_s (PO_3)
594,570 (m)	δ_s (PO_3)
460, 485, 512 (m)	δ_{as} (PO_3)

ν = stretching; δ = deformation; s = symmetric; as = asymmetric; w = weak; m = medium; s = strong.

Table 2
Crystallographic data and details of crystal structure refinement

Chemical formula	Mn H P O_3
Formula weight ($g\,mol^{-1}$)	134.92
Crystal system	Monoclinic
Space group	$P2_1/c$ (no. 14)
a (Å)	8.036(3)
b (Å)	8.240(3)
c (Å)	10.410(3)
β (°)	124.73(3)
V (Å^3)	566.5(3)
Z	8
ρ_{exp} ($g\,cm^{-3}$)	3.15(3)
ρ_{calc} ($g\,cm^{-3}$)	3.164
F 000)	520
$T(K)$	298
Radiation, λ(Mo-$K\alpha$) (Å)	0.71073
μ(Mo-$K\alpha$) (mm^{-1})	4.982
Measured reflections	3993
Independent	1238 [$R_{int} = 0.0281$]
Observed [$I > 2\sigma(I)$]	1086
R [$I > 2\sigma(I)$]	$R1 = 0.022$, w$R2 = 0.0526$
R [all data]	$R1 = 0.0266$, w$R2 = 0.0539$
Goodness of fit	1.009
Largest diff. Peak and hole (e Å^{-3})	0.751 and −0.410

$R1 = [\Sigma(|F_o| - |F_c|)]/\Sigma|F_o|$; $wR2 = [\Sigma[w(|F_o|^2 - |F_c|^2)^2]/\Sigma[w(|F_o|^2)^2]]^{1/2}$; $w = 1/\sigma^2|F_o|^2 + (xp)^2 + yp]$; where $p = [|F_o|^2 + 2|F_c|^2]/3$; $x = 0.353$; $y = 0.00$.

2.3. Physicochemical characterisation techniques

Atomic emission spectroscopy measurements were carried out on an ARL Fisons 3410 + ICP with a TH minitorch. The IR spectrum (KBr pellets) was obtained with a Nicolet FT-IR 740 spectrophotometer between 400 and 4000 cm^{-1}. Thermogravimetric analysis was carried out in a SDC 2960 Simultaneous DSC-TGA instrument, under synthetic air atmosphere. A crucible

with 20 mg of sample was heated at a rate of 5 °C/min from room temperature to 800 °C. Temperature dependent X-ray diffraction experiment has been carried out on a Philips X′PERT automatic diffractometer (Cu-$K\alpha$ radiation) equipped with a variable-temperature Anton Paar HTK16 Pt stage. Excitation and emission spectra were recorded with a SPEX Fluorolog 212 spectrofluorometer. The excitation spectrum was corrected for the variation of the incident flux and the emission spectrum for the transmission of the monochromator and the response of the photomultiplier. The reflectance spectrum was obtained with the same equipment by simultaneous rotation of the monochromators placed before and after the sample. Decay time measurements were performed with the SPEX Fluorolog-2 1934D phosphorimeter. The excitation source was a xenon lamp delivering microsecond pulses. ESR spectra were recorded by a Bruker ESP 300 spectrometer, using an Oxford Instrument (ITC 4) regulator to stabilise the temperature. Magnetic susceptibility measurements in the temperature range 5–300 K were performed on a powdered sample using a Quantum Design MPMS-7 SQUID magnetometer, under applied fields of 1000, 500 and 250 G, values in the range of linear dependence of magnetisation vs. magnetic field even at 5 K.

3. Results and discussion

3.1. Crystal structure

The structure of $Mn(HPO_3)$ consists of a three-dimensional compact framework formed by MnO_6 octahedra and $(HPO_3)^{2-}$ trigonal pyramids (Fig. 1). There are two crystallographically independent manganese and phosphorus atoms that give rise to two different octahedra and pyramids. Each $Mn(1)O_6$ coordination polyhedron is linked to an equivalent, via the edge formed by two O(4) atoms, and to two $Mn(2)O_6$ octahedra by the edges formed by O(6)–O(3) and O(1)–O(2) (Fig. 2a). Similarly, $Mn(2)O_6$ shares edges with three other octahedra: two $Mn(1)O_6$ via O(6)–O(3) and O(1)–O(2) edges, and to another $Mn(2)O_6$ via the edge formed by two O(2) atoms (Fig. 2b). This connectivity gives rise to a three-dimensional network of edge sharing octahedra in which the $[HP(1)O_3)]^{2-}$ pyramids share the O(2)–O(6) edge with the $Mn(1)O_6$ octahedra, and its third oxygen, O(1), also linked to Mn(1) and Mn(2) (Fig. 3a). $[HP(2)O_3]^{2-}$ pyramids therefore have a base formed by O(3), O(4) and O(5) that connects the P(2) atom to three Mn(1) and two Mn(2) atoms (Fig. 3b).

Table 3 gives atomic coordinates. Tables 4 and 5 show the selected bond distances and angles, respectively. The mean Mn–O distance for the $Mn(1)O_6$ octahedron is 2.2(2) Å, the *cis* O–Mn–O angles vary from 60.86(6)° to 128.43(7)° and the O–Mn–O *trans* angles from 135.87(6)° to 168.17(6)°. Metal-oxygen distances for the $Mn(2)O_6$ octahedron have the same mean value as $Mn(1)O_6$, but angles show less variation with *cis* angles from 75.28(6)° to 104.26(7)° and *trans* angles from 155.88(6)° to 178.50(6)°. Both coordination polyhedra are highly distorted from ideal octahedral towards trigonal prismatic geometry [12]: 37.6% for $Mn(1)O_6$ and 33.5% for $Mn(2)O_6$. The greater value of 37.6% of the Mn(1) octahedron is primarily due to the unusually large bond distance of 2.654(2) Å with O(2). Phosphite groups present mean P–O bond lengths of 1.531(7) Å for P(1) and 1.52(2) Å for P(2), and P–H bond distances of 1.35(3) and 1.29(3) Å respectively. Angles are between 108.0(1) and 114.27(9)° in the $[HP(1)O_3]^{2-}$ pyramid and range from 110.6(1) to 113.3(1)° for $[HP(2)O_3]^{2-}$.

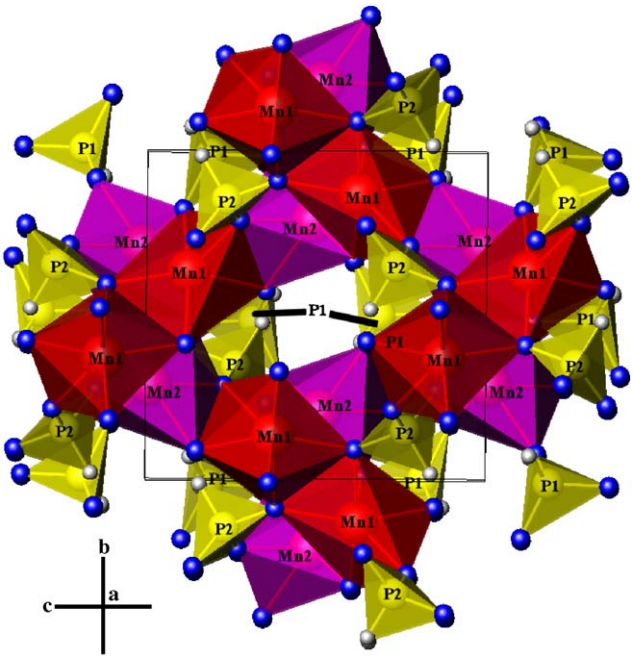

Fig. 1. Crystal structure of $Mn(HPO_3)$.

Bond valence [13] calculations have been performed for Mn^{2+} cations and $(PH)^{4+}$ groups [14] obtaining values of 2.01 and 1.97 v. u. for Mn(1) and Mn(2), and 3.88 and 3.99 for $[P(1)H]^{4+}$ and $[P(2)H]^{4+}$, respectively.

3.2. Thermal study

The DTA curve shows a highly exothermic process at 580 °C coincident in temperature with a sharp peak in the TG curve. This is due to the following oxidative reaction: $2 \cdot Mn(HPO_3) + O_2 \rightarrow Mn_2P_2O_7 + H_2O$, in which one molecule of water per formula is formed and lost, and manganese pyrophosphate crystallises. The total mass loss during the reaction was approximately 1%. The residue, characterized by X-ray powder diffraction, showed $Mn_2P_2O_7$ ($C2/m$, $a = 6.636$ Å, $b = 8.584$ Å,

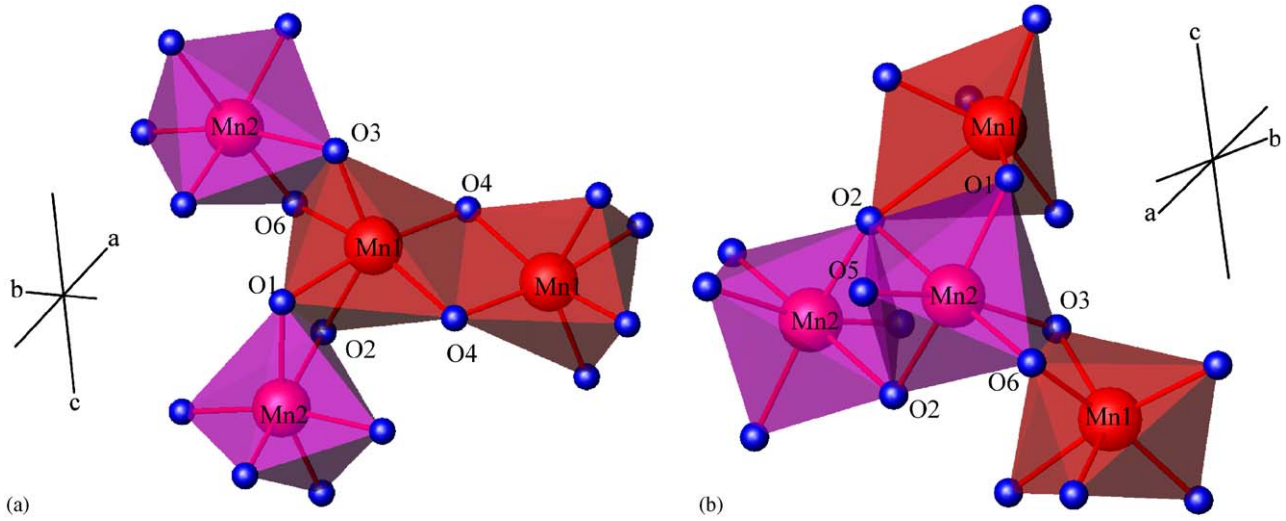

Fig. 2. Connectivity of (a) the Mn(1) and (b) the Mn(2) coordination polyhedra.

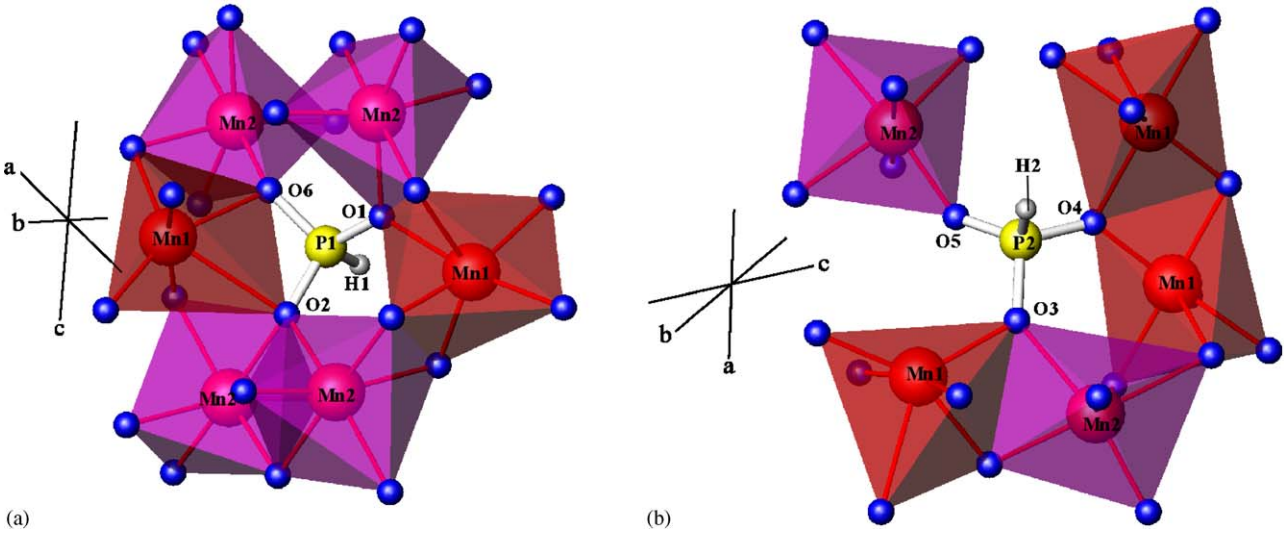

Fig. 3. Connectivity of (a) the $[HP(1)O_3]^{2-}$ and (b) the $[HP(2)O_3]^{2-}$ phosphite groups.

Table 3
Fractional atomic coordinates and equivalent isotropic thermal parameters, U_{eq} ($Å^3 \times 10^3$) (e.s.d. in parentheses)

Atom	x/A	Y/B	Z/C	U_{eq}
Mn(1)	0.8196(1)	−0.3683(1)	−0.1241(1)	13(1)
Mn(2)	0.4744(1)	−0.7899(1)	−0.5132(1)	11(1)
P(1)	0.4074(1)	−0.5092(1)	−0.3141(1)	10(1)
P(2)	−0.0502(1)	−0.8516(1)	−0.7649(1)	11(1)
O(1)	0.3512(3)	−0.6760(2)	−0.3932(2)	14(1)
O(2)	0.5175(3)	−0.5153(2)	−0.1355(2)	13(1)
O(3)	0.1528(2)	−0.7890(2)	−0.7268(2)	15(1)
O(4)	−0.0285(2)	−0.9093(2)	−0.6158(2)	17(1)
O(5)	0.7848(3)	−0.7707(2)	−0.3555(2)	21(1)
O(6)	0.5410(2)	−0.4169(2)	−0.3496(2)	14(1)

$U_{eq} = (1/3)[U_{33} + 1/\sin^2\beta(U_{11} + U_{33} + 2U_{13}\cos\beta)]$.

$c = 4.545$ Å and $\beta = 102.78°$) [15] to be the only phase present in it.

Temperature dependent X-ray diffraction studies (Fig. 4) have also been performed to determine the thermal stability of $Mn(HPO_3)$. Powder patterns were recorded from 30 to 810 °C every 15 °C in the $5° \leqslant 2\theta \leqslant 38.5°$ rangewith an integration time of 1 s per 0.03° step. $Mn(HPO_3)$ is stable up to 580 °C, at which temperature there is a rapid transition to $Mn_2P_2O_7$.

3.3. Luminescence and UV-vis spectroscopies

The photoluminescence studies of $Mn(HPO_3)$ have shown that the luminescence of manganese is not totally quenched at room temperature, there being a red

Table 4
Selected bond distances (Å) for $Mn(HPO_3)$

$Mn(1)O_6$ octahedron	
$Mn(1)–O(4)^{i}$	2.095(2)
$Mn(1)–O(3)^{ii}$	2.129(2)
Mn(1)–O(6)	2.167(2)
$Mn(1)–O(1)^{i}$	2.170(2)
$Mn(1)–O(4)^{iii}$	2.176(2)
Mn(1)–O(2)	2.654(2)
$Mn(2)O_6$ octahedron	
Mn(2)–O(5)	2.068(2)
$Mn(2)–O(6)^{ii}$	2.181(2)
Mn(2)–O(1)	2.198(2)
$Mn(2)–O(2)^{iv}$	2.196(2)
Mn(2)–O(3)	2.253(2)
$Mn(2)–O(2)^{v}$	2.395(2)
$HP(1)O_3$ trigonal pyramid	
P(1)–O(6)	1.524(2)
P(1)–O(1)	1.532(2)
P(1)–O(2)	1.538(2)
P(1)–H(1)	1.35(3)
$HP(2)O_3$ trigonal pyramid	
$P(2)–O(5)^{vi}$	1.496(2)
P(2)–O(3)	1.532(2)
P(2)–O(4)	1.535(2)
P(2)–H(2)	1.29(3)

Symmetry codes: i = $-x+1$, $y+1/2$, $-z-1/2$; ii = $-x+1,-y-1$, $-z-1$; iii = $x+1,-y-3/2,z+1/2$; iv = $x,-y-3/2$, $z-1/2$; v = $-x+1$, $y-1/2,-z-1/2$; vi = $x-1,-y-3/2$, $z-1/2$.

Table 5
Selected bond angles (deg) of $Mn(HPO_3)$

$Mn(1)O_6$ octahedra	
$O(4)^{i}–Mn(1)–O(3)^{ii}$	128.43(7)
$O(4)^{i}–Mn(1)–O(6)$	153.27(7)
$O(3)^{ii}–Mn(1)–O(6)$	78.17(7)
$O(4)^{i}–Mn(1)–O(1)^{i}$	97.72(7)
$O(3)^{ii}–Mn(1)–O(1)^{i}$	87.08(7)
$O(6)–Mn(1)–O(1)^{i}$	84.99(7)
$O(4)^{i}–Mn(1)–O(4)^{iii}$	76.50(7)
$O(3)^{ii}–Mn(1)–O(4)^{iii}$	104.62(7)
$O(6)–Mn(1)–O(4)^{iii}$	95.60(7)
$O(1)^{i}–Mn(1)–O(4)^{iii}$	168.17(6)
$O(4)^{i}–Mn(1)–O(2)$	94.09(7)
$O(3)^{ii}–Mn(1)–O(2)$	135.87(6)
O(6)—Mn(1)–O(2)	60.86(6)
$O(1)^{i}–Mn(1)–O(2)$	74.43(6)
$O(4)^{iii}$—Mn(1)–O(2)	95.50(6)
$Mn(2)O_6$ octahedra	
$O(5)–Mn(2)–O(6)^{ii}$	93.05(7)
O(5)–Mn(2)–O(1)	104.26(7)
$O(6)^{ii}–Mn(2)–O(1)$	99.38(6)
$O(5)–Mn(2)–O(2)^{iv}$	89.93(7)
$O(6)^{ii}–Mn(2)–O(2)^{iv}$	99.22(7)
$O(1)–Mn(2)–O(2)^{iv}$	155.88(6)
O(5)–Mn(2)–O(3)	165.93(7)
$O(6)^{ii}–Mn(2)–O(3)$	75.28(6)
O(1)–Mn(2)–O(3)	85.68(7)
$O(2)^{iv}–Mn(2)–O(3)$	84.33(7)
$O(5)–Mn(2)–O(2)^{v}$	88.25(7)
$O(6)^{ii}–Mn(2)–O(2)^{v}$	178.50(6)
$O(1)–Mn(2)–O(2)^{v}$	79.57(6)
$O(2)^{iv}–Mn(2)–O(2)^{v}$	81.51(7)
$O(3)–Mn(2)–O(2)^{v}$	103.525(6)
$HP(1)O_3$ trigonal pyramid	
O(6)–P(1)–O(1)	110.49(9)
O(6)–P(1)–O(2)	108.04(10)
O(1)–P(1)–O(2)	114.27(9)
O(6)–P(1)–H(1)	109(1)
O(1)–P(1)–H(1)	108(1)
O(2)–P(1)–H(1)	107(1)
$HP(2)O_3$ trigonal pyramid	
$O(5)^{vi}–P(2)–O(3)$	111.5(1)
$O(5)^{vi}–P(2)–O(4)$	113.3(1)
O(3)–P(2)–O(4)	110.6(1)
$O(5)^{vi}–P(2)–H(2)$	111(1)
O(3)–P(2)–H(2)	104(1)
O(4)–P(2)–H(2)	106(1)

Symmetry codes: i = $-x+1,y+1/2,-z-1/2$; ii = $-x+1,-y-1,-z-1$; iii = $x+1,-y-3/2,z+1/2$; iv = $x,-y-3/2,z-1/2$; v = $-x+1,y-1/2,-z-1/2$; vi = $x-1,-y-3/2,z-1/2$.

emission associated to an octahedral coordination of the Mn^{2+} (d^5).

The excitation spectrum (Fig. 5) is constituted of different groups of absorption bands. The band located around 250 nm is associated with the charge transfer state of Mn^{2+}–O^{2-}. Those ranging from 300 to 580 nm correspond to the forbidden $3d \rightarrow 3d$ transitions of manganese, the bands located between 300 and 340 nm being components of the $^4E(^4D)$ levels and those between 340 and 380 nm of the $^4T_2(^4D)$ level. The sharp lines observed at 406 and 412 nm arise from the splitting of the $^4A_1,^4E(^4G)$ levels. This splitting reflects the reduction of the crystal field symmetry, with highly distorted MnO_6 octahedra, as previously discussed. Finally, two broad bands between 420 and 520 nm are associated with components of the $^4T_2(^4G)$ and $^4T_1(^4G)$ levels. All these bands can be identified on the diffuse reflectance spectrum (Fig. 5) and are coincident with those reported in the literature [1,3b,3c,16]. Racah ($B = 910$ and $C = 3135\,cm^{-1}$) and Dq ($820\,cm^{-1}$) parameters have been calculated showing a minimal covalent character since the B-value is approximately 95% of the corresponding to the free Mn^{2+} cation ($960\,cm^{-1}$) [17].

The emission spectrum (Fig. 6), performed for an excitation at 412 nm, shows a broad emission band with halfwidth of approximately 80 nm, assigned to the $^4T_1(^4G) \rightarrow {}^6A_1(^6S)$ transition at 650 nm. This red emission is as expected for the octahedral coordination of manganese described previously. The associated trichromatic coordinates are $x = 0.672$ and $y = 0.3$, which correspond to a red colour according to the Commission Internationale de l'Eclairage chromaticity graph [18].

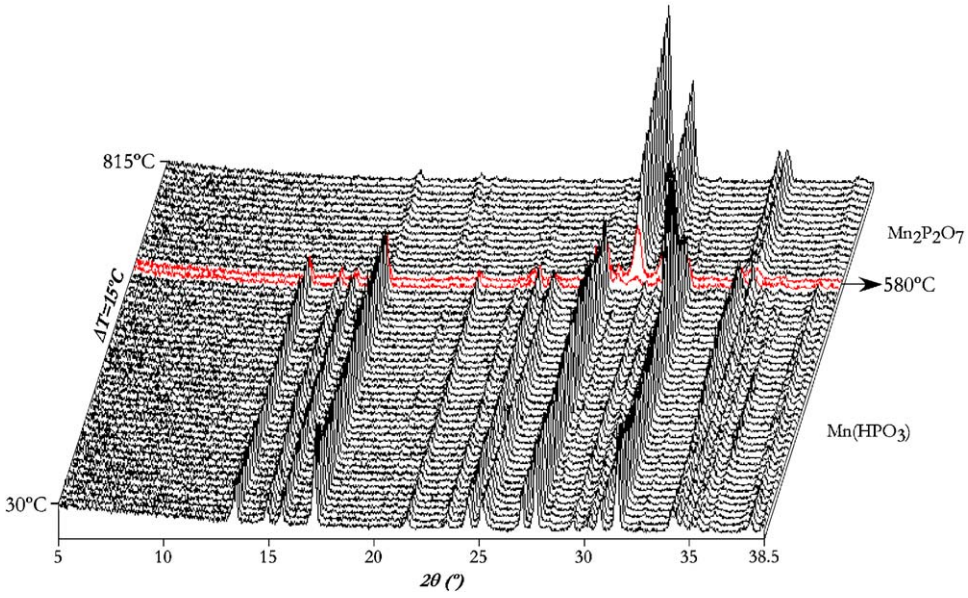

Fig. 4. Temperature dependent X-ray diffraction study.

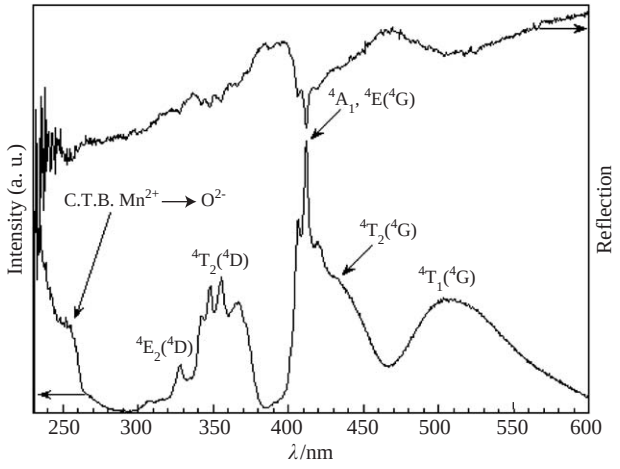

Fig. 5. Excitation spectrum for an emission at 650 nm (lower) and diffuse reflectance spectrum (upper) of $Mn(HPO_3)$.

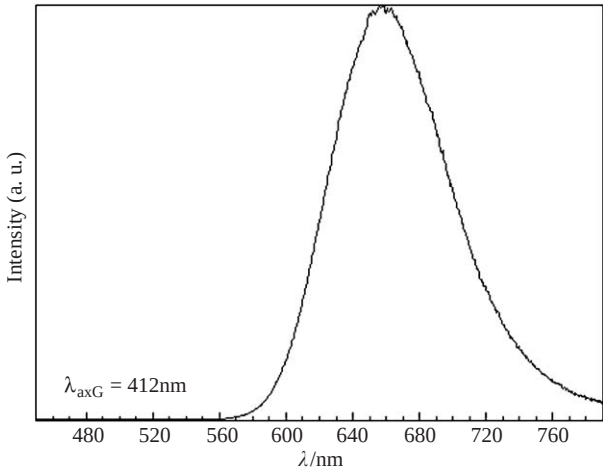

Fig. 6. Emission band of $Mn(HPO_3)$ for an excitation at 412 nm.

The Stokes shift, the difference between the maximum of the emission and the corresponding excitation, is equal to approximately 4400 cm^{-1}.

The decay time, measured at $\lambda_{exc} = 412$ nm and $\lambda_{em} = 650$ nm, indicates the non-negligible contribution of the non-radiative transitions in the de-excitation process. The fit to the data shows an equivalent contribution of two exponential components, corresponding to first and second decay times, τ_1 and τ_2 of 556 and 125 μs. A significant part of the radiative emission may be lost due to concentration quenching as the concentration of manganese in this phase is equal to 1.4×10^{22} ions/cm^3.

3.4. ESR and magnetic behavior

ESR spectra were performed at the X-band on a powdered sample at temperatures between 290 and 4.2 K (Fig. 7). The spectra exhibit isotropic signals due to the presence of coupled Mn(II) cations in octahedral coordination with a g-value of 2.00(1). Below 20 K the signals broaden and lose intensity. The thermal dependence of the linewidth and the intensity are shown in Fig. 8. There is a slight increase of the linewidth from 290 to 100 K, temperature from which the increase is more rapid due to spin correlation [19]. The linewidth reaches a maximum at 16 K and decreases until 10 K where there is a minimum whereas the intensity

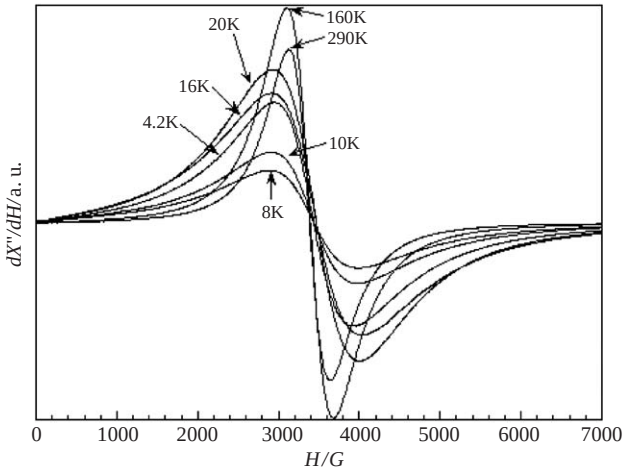

Fig. 7. ESR signals for $Mn(HPO_3)$ at different temperatures

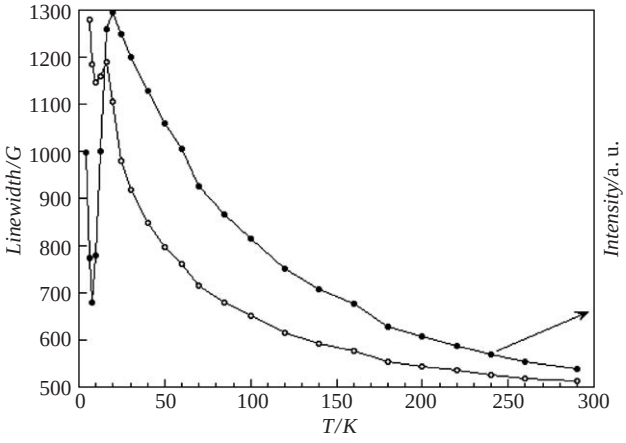

Fig. 8. Thermal evolution of the intensity and linewidth for $Mn(HPO_3)$.

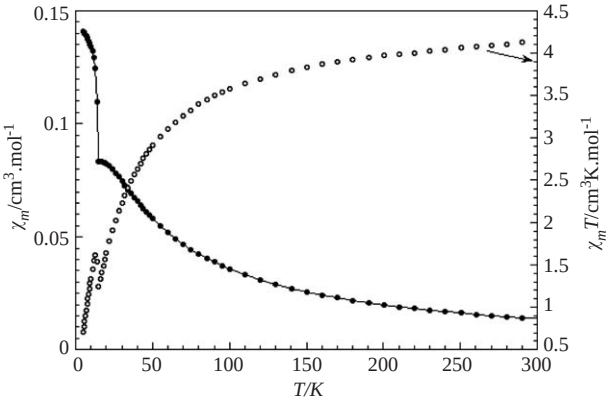

Fig. 9. Thermal variation of χ_m and $\chi_m T$ at 1000 G.

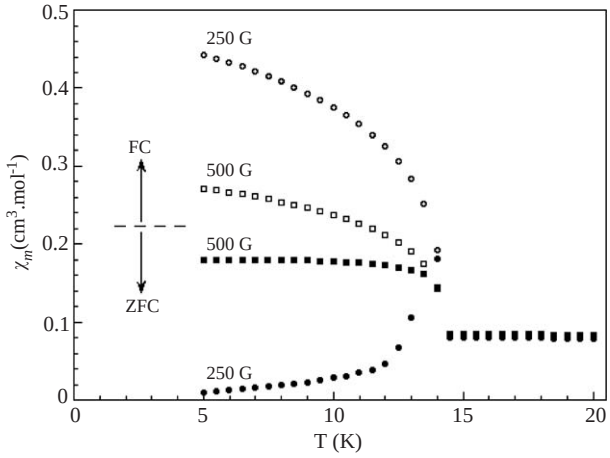

Fig. 10. Irreversibility of ZFC and FC χ_m curves at 500 and 250 G.

increases continuously on lowering the temperature until 20 K, where there is a maximum. At 8 K the intensity reaches a minimum and increases again down to 4.2 K. The variation of the linewidth as well as the sudden increase of the intensity can be attributed to a ferromagnetic component probably associated with a spin canting phenomenon below 8 K.

Magnetic measurements of $Mn(HPO_3)$ were performed on a powdered sample from 5 K to room temperature. The thermal evolution of χ_m and $\chi_m T$ curves under an applied field of 1000 G, are shown in Fig. 9. The thermal variation of the molar magnetic susceptibility follows the Curie–Weiss law [$\chi_m = C_m/(T-\theta)$] above ca. 30 K with values of the Curie and Curie–Weiss constants of 4.5 $cm^3\,K\,mol^{-1}$ and −27.8 K, respectively. At temperatures below 15 K, a sudden increase of both χ_m and $\chi_m T$ is observed, with $\chi_m T$ reaching a maximum at 12 K. *Zero field cooling* and *field cooling* magnetic susceptibility curves measured at 1000 G show irreversibility below 14 K. Lowering the applied field to 500 and 250 G produced a greater separation between *zero field cooling* and *field cooling* curves (Fig. 10).

Magnetisation vs magnetic field measurements (Fig. 11) at 5 K showed hysteresis corroborating a ferromagnetic component at this temperature. The values of the remanent magnetisation and coercive field are 100 $cm^3\,mol^{-1}$ and 1300 G. There is no remanent magnetisation observed at 15 K after cooling the sample under a magnetic field of 250 G (Fig. 12).

These results confirm a significant ferromagnetic component at low temperatures below 15 K, attributed to a canting of the antiferromagnetically aligned spins.

In the three-dimensional framework formed by edge sharing MnO_6 octahedra and $(HPO_3)^{2-}$ pyramids (Figs. 2 and 3), three different magnetic exchange pathways can take place: (i) direct intermetallic interactions between manganese (II) cations via d_{xy}, d_{xz} and d_{yz} orbitals that lead to antiferromagnetic couplings; (ii) superexchange Mn–O–Mn interactions involving metal

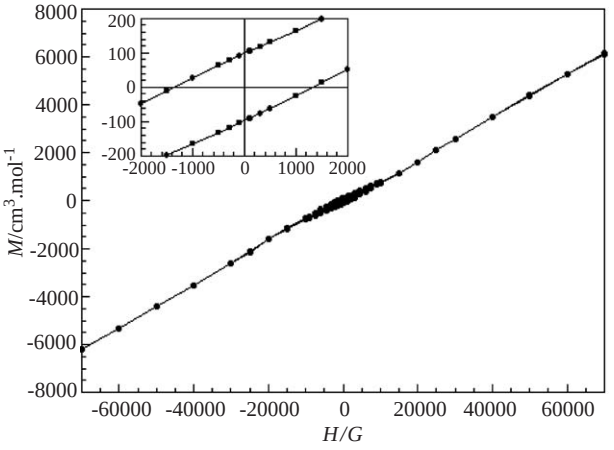

Fig. 11. Magnetisation (M) vs. applied field (H) for $Mn(HPO_3)$ at 5 K. Detail of the low field (−2000 to 2000 G) region is inset.

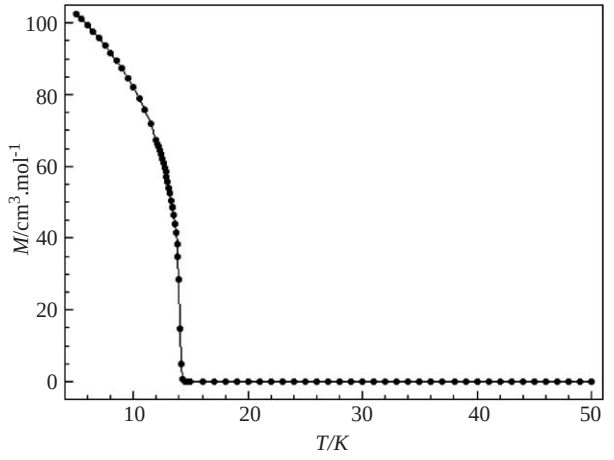

Fig. 12. Remanent magnetisation vs. temperature of $Mn(HPO_3)$.

d_z2, d_x2-_y2 orbitals between edge sharing octahedra. Considering the angles shown in Table 6, both ferro- and antiferromagnetic interactions can take place [20]; (iii) superexchange interactions through $(HPO_3)^{2-}$ groups contributing to the antiferromagnetic couplings. The competition between these three magnetic exchange pathways in $Mn(HPO_3)$ produce interactions that are of antiferromagnetic nature with a remanent magnetic moment below 15 K due to spin canting.

The $(NH_4)[Mn(XO_4)]\cdot H_2O$ ($X =$ P and As) bidimensional "dittmarite"-type compounds also show an antiferromagnetic behavior with a spin canting phenomenon, observed from the thermal evolution of the molar magnetic susceptibility at different values of magnetic field. For the phosphate phase, the J-exchange parameter is $J/k = -1.6$ K, whereas the J-value for the arsenate-dittmarite was estimated as −0.9 K by using the molecular field theory [21].

Table 6
Intermetallic Mn–Mn distances (Å) and selected angles (deg) of the possible magnetic exchange pathways for $Mn(HPO_3)$

Mn–Mn distances	
Mn(1)–Mn(1)^{ii}	3.355(1)
Mn(1)–Mn(2)^{v}	3.373(1)
Mn(1)–Mn(2)	3.448(1)
Mn(2)–Mn(2)^{ii}	3.480(1)
Mn–O–Mn angles	
Mn(1)^{v}–O(1)–Mn(2)	104.25(7)
Mn(1)^{ii}–O(3)–Mn(2)	100.61(7)
Mn(1)–O(6)–Mn(2)^{ii}	101.74(7)
Mn(1)^{v}–O(4)–Mn(1)^{vi}	103.50(7)
Mn(2)^{vii}–O(2)–Mn(1)	138.59(8)
Mn(2)^{i}–O(2)–Mn(1)	85.97(5)
Mn(2)^{vii}–O(2)–Mn(2)^{i}	98.49(7)

Symmetry codes: i = $-x+1,y+1/2,-z-1/2$; ii = $-x+1,-y-1,-z-1$; v = $-x+1,y-1/2,-z-1/2$; vi = $x-1$, $-y-3/2$, $z-1/2$; vii = $x,-y-3/2$, $z+1/2$.

4. Concluding remarks

A new manganese (II) phosphite has been synthesised under mild hydrothermal conditions. The structure consists of a three-dimensional, compact framework formed by edge sharing MnO_6 octahedra linked by oxygens to $(HPO_3)^{2-}$ phosphite groups. The presence of two δ(P–H) bands in the IR spectrum is consistent with the existence of two crystallographically independent phosphite groups in the structure. This phase has a high thermal stability, 580 °C, that leads to a transformation by an oxidative reaction with the loss of one water molecule per formula. Photoluminescence studies revealed a red emission consistent with the octahedral coordination of the manganese cations. ESR spectra are isotropic with a g-value of 2.00(1). The magnetic behavior of $Mn(HPO_3)$ appears to be antiferromagnetic from room temperature to 15 K, temperature at which a ferromagnetic transition takes place due to a spin canting.

Acknowledgments

This work has been financially supported by the "Ministerio de Educación y Ciencia" (MAT2004-02071), the "Universidad del País Vasco" (UPV/EHU) (9/UPV00130.310-15967/2004 and 9/UPV00169.310-13494/2001) and the "Fondo Europeo de Desarrollo Regional". We thank Dr. J. P. Chapman and Dr. I. Orue ("Fondo Europeo Social" and "Ministerio de Ciencia y Tecnología") for the X-ray diffraction and magnetic measurements, respectively. U-Chan Chung thanks the UPV/EHU for funding.

References

[1] (a) S.M. Kauzlarich, P.K. Dorhout, J.M. Honig, J. Solid State Chem. 149 (2000) 3;
(b) C.N.R. Rao, J. Gopalakrihnan, New Directions in Solid State Chemistry. Structure, Synthesis, Properties, Reactivity and Materials Design, Cambridge University Press, Cambridge, 1986.

[2] G. Bonavia, J. DeBord, R.C. Haushalter, D. Rose, J. Zubieta, Chem. Mater. 7 (1995) 1995.

[3] (a) S. Fernandez, J.L. Mesa, J.L. Pizarro, L. Lezama, M.I. Arriortua, R. Olazcuaga, T. Rojo, Chem. Mater. 12 (8) (2000) 2092;
(b) S. Fernandez, J.L. Mesa, J.L. Pizarro, L. Lezama, M.I. Arriortua, R. Olazcuaga, T. Rojo, Inorg. Chem. 40 (14) (2001) 3476;
(c) S. Fernandez, J.L. Pizarro, J.L. Mesa, L. Lezama, M.I. Arriortua, T. Rojo, Int. J. Inorg. Mater 3 (4–5) (2001) 331;
(d) W.T.A. Harrison, J. Solid State Chem. 160 (1) (2001) 4;
(e) W.T.A. Harrison, M.L.F. Phillips, T.M. Nenoff, J. Chem. Soc. Dalton Trans. 17 (2001) 2459;
(f) W.T.A. Harrison, M.L.F. Phillips, T.M. Nenoff, Int. J. Inorg. Mater 3 (7) (2001) 1033;
(g) S. Fernandez, J.L. Mesa, J.L. Pizarro, L. Lezama, M.I. Arriortua, T. Rojo, Angew. Chem. Int. Ed. 41 (19) (2002) 3683;
(h) S. Fernandez, J.L. Mesa, J.L. Pizarro, L. Lezama, M.I. Arriortua, T. Rojo, Chem. Mater. 14 (5) (2002) 2300;
(i) M.L.F. Phillips, T.M. Nenoff, C.T. Thompson, W.T. A Harrison, J. Solid State Chem. 167 (2002) 333;
(j) W.T.A. Harrison, R.M. Yeates, M.L.F. Phillips, T.M. Nenoff, Inorg. Chem. 42 (5) (2003) 1493;
(k) W.T.A. Harrison, Solid State Sci 5 (2) (2003) 297;
(l) J. Liang, Y. Wang, J. Yu, Y. Li, R. Xu, Chem. Comm. 7 (2003) 882;
(m) W. Dong, G. Li, Z. Shi, W. Fu, D. Zhang, X. Chen, Z. Dai, L. Wang, S. Feng, Inorg. Chem. Comm. 6 (6) (2003) 776;
(n) U. Chung, J.L. Mesa, J.L. Pizarro, L. Lezama, J.S. Garitaonandia, J.P. Chapman, M.I. Arriortua, J. Solid State Chem. 177 (8) (2004) 2705;
(o) J.A. Johnstone, W.T.A. Harrison, Inorg. Chem. 43 (15) (2004) 4567;
(p) S. Shi, Q. Wei, G. Li, W. Li, H. Yuan, J. Xu, G. Zhu, T. Song, S. Qiu, J. Solid State Chem. 177 (9) (2004) 3038;
(q) S. Fernandez, J.L. Mesa, J.L. Pizarro, J.S. Garitaonandia, M.I. Arriortua, T. Rojo, Angew. Chem. Int. Ed. 43 (8) (2004) 977.

[4] (a) D.E.C. Corbridge, Acta Crystallogr 9 (1956) 991;
(b) M. Handlovic, Acta Crystallogr. B 25 (1969) 227;
(c) R.H. Colton, D.E. Henn, J. Chem. Soc. A 9 (1971) 1207;
(d) F. Petru, A. Muck, Collection Czech. Chem. Comm. 36 (11) (1971) 3774;
(e) M. Rafiq, J. Durand, L. Cot, C. R. Acad. Sci. Ser. C 288 (15) (1979) 411
(f) J. Loub, H. Paulus, Acta Crystallogr. B 37 (1106).;
(g) M. Ebert, L. Kaban, J. Less-Common Met. 81 (1) (1981) 55;
(h) M. Rafiq, J. Durand, L. Cot, Rev. Chim. Miner. 18 (1) (1981) 1;
(i) J. Brynda, B. Kratochvil, I. Cisarova, Collection Czech. Chem. Comm. 52 (7) (1987) 1742;
(j) C.Y. Ortiz-Avila, P.J. Squattrito, M. Shieh, A. Clearfield, Inorg. Chem. 28 (1989) 2608;
(k) M.D. Marcos, P. Gomez-Romero, P. Amoros, F. Sapina, D. Beltran-Porter, R. Navarro, C. Rillo, F. Lera, J. Appl. Phys. 67 (9) (1990) 5998;
(l) M. Sghyar, J. Durand, L. Cot, M. Rafiq, Acta Crystallogr. C 47 (1991) 2515;
(m) M.D. Marcos, P. Amoros, A. Beltrán-Porter, R. Martinez-Manez, J.P. Attfield, Chem. Mater. 5 (1) (1993) 121;
(n) M.D. Marcos, P. Amoros, F. Sapiña, A. Beltrán-Porter, R. Martinez-Manez, J.P. Attfield, Inorg. Chem. 32 (23) (1993) 5044;
(o) J.D. Foulon, N. Tijani, J. Durand, M. Rafiq, L. Cot, Acta Crystallogr. C 49 (1993) 1;
(p) M.D. Marcos, P. Amoros, A. LeBail, J. Solid State Chem. 107 (1) (1993) 250;
(q) J.D. Foulon, N. Tijani, J. Durand, M. Rafiq, L. Cot, Acta Crystallogr. C 49 (1993) 849;
(r) R.E. Morris, M.P. Attfield, A.K. Cheetham, Acta Crystallogr. C 50 (1994) 473;
(s) M.P. Attfield, R.E. Morris, A.K. Cheetham, Acta Crystallogr. C 50 (1994) 981;
(t) A.H. Mahmoudkhani, V. Langer, Phosphorus Sulfur Silicon Relat. Elem. 176 (2001) 83;
(u) B. Ewald, Y. Prots, R. Kniep, Z. Kristallogr.—New Cryst. Struct. 218 (4) (2003) 377;
(v) R. Ouarsal, R. Essehli, M. Lachkar, M. Zenkouar, M. Dusek, K. Fejfarova, B. El Bali, Acta Crystallogr. E 60 (2004) 166.

[5] P. Román, J.M. Gutiérrez-Zorrilla, J. Chem. Educ. 62 (1985) 167.

[6] (a) M. Tsuboi, J. Am. Chem. Soc. 79 (1957) 1351;
(b) G. Bonavia, J. DeBord, R.C. Haushalter, D. Rose, J. Zubieta, Chem. Mater. 7 (1995) 1995;
(c) S. Fernandez, J.L. Pizarro, J.L. Mesa, L. Lezama, M.I. Arriortua, T. Rojo, Chem. Mater. 15 (2003) 1204.

[7] CRYSALIS version 1.170: Program for the Data Reduction, Oxford Diffraction Ltd., Oxford, England 2003.

[8] A. Altomare, G. Cascarano, C. Giacovazzo, A. Guagliardi, SIR 92: a program for crystal structure solution, J. Appl. Crystallogr. 26 (1993) 343.

[9] G.M. Sheldric, SHELXS97: Program for the Refinement of Crystal Structures, University of Göttingen, Germany, 1997.

[10] International Tables for X-ray Crystallography, vol VI, Kynoch Press, Birmingham, England, 1974, p. 99.

[11] E. Dowty, ATOMS: A Computer Program for Displaying Atomic Structures, Shape Software, 512 Hidden Valley Road, Kingsport, TN, 1993.

[12] E.L. Muetterties, L.J. Guggenberger, J. Am. Chem. Soc. 96 (1974) 1748.

[13] I.D. Brown, D. Altermatt, Acta Crystallogr. B 41 (1985) 244.

[14] (a) N.E. Brese, M. O′Keeffe, Acta Crystallogr. B 47 (1991) 192;
(b) J. Loub., Acta. Crystallogr. B 47 (1991) 468.

[15] Powder Diffraction Files Inorganic and Organic ICDD, No. 29-0891.

[16] (a) K.E. Lawson, J. Chem. Phys. 44 (1966) 4159;
(b) J. Escobal, J.L. Mesa, J.L. Pizarro, L. Lezama, R. Olazcuaga, T. Rojo, J. Mater. Chem. 9 (10) (1999) 2691;
(c) J. Escobal, J.L. Pizarro, J.L. Mesa, L. Lezama, R. Olazcuaga, M.I. Arriortua, T. Rojo, Chem. Mater. 12 (2) (2000) 376.

[17] A.B.P. Lever, Inorganic Electronic Spectroscopy, Elsevier Science Publishers B. V., Amsterdam, Netherlands, 1984.

[18] (a) R. Seve, Physique de la Couleur, Collection Physique Fondamentale et Appliquée, Masson, 1996
(b) M. Deribere, La Couleur-Que Sais-je, Presses Universitaires de France, 1996.

[19] (a) P.M. Richards, M.B. Salamon, Phys. Rev. B 9 (1974) 32;
(b) A. Bencini, D. Gatteschi, EPR of Exchange Coupled Systems, Springer-Verlag, Berlin, 1990.

[20] J.B. Goodenough, Magnetism and the Chemical Bond, New York Intersciences, 1963.

[21] (a) S.G. Carling, P. Day, D. Visser, Inorg. Chem. 34 (1995) 3917;
(b) J.L. Mesa, J.L. Pizarro, L. Lezama, A. Goñi, M.I. Arriortua, T. Rojo, Mat. Res. Bull. 34 (1999) 1545.